Design and In vitro Characterization of a Wearable Multisensing System for Hydration Monitoring

Sarah Tonello, *Member, IEEE*, Alberto Zacchini, Alessandra Galli, *Member, IEEE*, Ata Golparvar, *Member, IEEE*, Ali Meimandi, *Graduate Student Member, IEEE*, Giacomo Peruzzi, *Member, IEEE*, Alessandro Pozzebon, *Senior Member, IEEE*, Nicolò Lago, *Member, IEEE*, Andrea Cester, *Senior Member, IEEE*, Giada Giorgi, *Member, IEEE*, Sandro Carrara, *Fellow, IEEE*, and Claudio Narduzzi, *Life Member, IEEE*

***Abstract*— Dehydration is a frequent condition in the elderly and can lead to serious health complications if not compensated timely. Early diagnosis can be problematic, as medical examinations in the hospital would be needed. Fully wearable low-cost multisensing devices for home use could help investigate and prevent critical conditions. We introduce a sensing platform designed for operation in remote healthcare for the elderly. It combines a low-cost, highly customizable flexible inkjet-printed multisensor bracelet, including sensors for body impedance, skin hydration, and temperature monitoring, with a small, low-power front-end circuit and an embedded unit that communicates by a Low Power Wide Area Network (LoRaWAN) transmission interface. We describe individual system components and present in vitro experiments for their characterization. Reported results represent the fundamental proof of concept for the development of a fully operating device that can be used satisfactorily to monitor dehydration in a real-life application scenario.**

***Index Terms*— Active aging, bioelectrical impedance analysis (BIA), hydration monitoring, in vitro characterization, inkjet printing.**

I. Introduction

DEHYDRATION occurs whenever water balance in the human body is negative, that is, water intake is less than its output. It is a common reason why elderly patients come to emergency departments, affecting quality of life and involving a significant economic burden for the healthcare system. Moderate dehydration may cause headache, confusion, fatigue, dizziness, weakness, delirium, and high heart rate correlated with low blood pressure. If not compensated, it can develop into severe complications and eventual death [1].

Manuscript received 10 November 2023; accepted 10 January 2024. Date of publication 27 February 2024; date of current version 7 March 2024. This work was supported in part by the "DEI Proactive 2018" Project ("Fully Printed Organic Array of Bidirectional Reference-Less Sensors for Neuronal Interfacing"); in part by the Networking Project ("Smart Wearable Sensors for E-Health Applications") funded by the Department of Information Engineering, University of Padua; and in part by the European Union under the Italian National Recovery and Resilience Plan (NRRP) of NextGenerationEU, PRIN 2022 Project 2022EKEFX8 - "Investigating the 5G-IoT paradigm shift in wireless-sensing based measurement applications for workplace safety." The Associate Editor coordinating the review process was Dr. Xun Chen. *(Corresponding author: Sarah Tonello.)*

Sarah Tonello, Alberto Zacchini, Alessandra Galli, Giacomo Peruzzi, Alessandro Pozzebon, Nicolò Lago, Andrea Cester, Giada Giorgi, and Claudio Narduzzi are with the Department of Information Engineering, University of Padua, I-35131 Padua, Italy (e-mail: sarah.tonello@unipd.it).

Ata Golparvar, Ali Meimandi, and Sandro Carrara are with the Bio/CMOS Interfaces Laboratory (BCI), École Polytechnique Fédérale de Lausanne (EPFL), 2000 Lausanne, Switzerland.

Digital Object Identifier 10.1109/TIM.2024.3369161

Although dehydration may be occasionally assessed at home or during ambulatory visits, accurate medical evaluation involves advanced instrumentation, laboratory analyses, and specialized medical staff. In most cases, it is only diagnosed when the elderly are admitted to the hospital under already severe conditions. This problem motivated researchers to focus on the development of home monitoring devices for early detection of dehydration, requiring no specialized personnel support [2]. A portable sensor that can simultaneously monitor sweat rate/loss, pH, lactate, glucose, and chloride was proposed in [3]. At specific time instants the user is required to take a photograph of the sensor, which is then digitally processed to assess hydration status. However, many elders do not possess enough skill and/or physical strength to use a smartphone. In [4], a chemical sensor platform was proposed to measure potassium concentration in urine. This is only limited to urination events and does not apply to continuous monitoring. In another example, the conductance of saliva is measured to assess the occurrence of dehydration, but saliva samples are easily contaminated by diet and even by simply talking [5]. All these approaches require active collaboration and some ability by the user, and therefore their suitability for elderly healthcare is questionable [6].

In our work, we aim at a compact, user-friendly, and fully autonomous Internet of Things (IoT)-based system that can reliably monitor multiple hydration-related parameters. A wireless IoT interface can be employed to relay alerts to healthcare providers. The system should be wearable, noninvasive, and require no active user involvement, enabling elderly users to carry on with normal daily activities and move freely in and out of their home environment.

Following and extending our previous literature overview of existing technologies presented in [7], we propose here the design and characterization of an integrated platform that can measure physiological quantities related to body hydration using comfortable, low-cost, and customized ink-jet printed electrodes and sensors. The sensor set is the result of a tradeoff between medical relevance and ease of noninvasive monitoring, which led to the choice of three sensed quantities from which full hydration parameters could be estimated: body impedance, local surface impedance, and local temperature.

In this article, we introduce some linear approximations to show that relationships between the previous quantities and the global water content in the body and surface skin hydration

do exist. However, such a simplified model may easily prove unsatisfactory in a practical application. Better results could be expected by inferring information about global water content and surface skin hydration through a suitable machine-learning (ML) algorithm. This part will be considered in the final release of the proposed wearable system, while in this article we focus the attention on the hardware design. The final goal of the designed sensing system is to provide early warning of impending dehydration in the elderly. For this purpose, a simple ordinal scale related to the severity of dehydration (e.g., null, moderate, significant, and severe) can suffice and accurate measurement of body water content is beyond the present scope of our work.

Results obtained from in vitro characterization of each sensor are discussed in this work, as well as tests of the reliability and robustness of signal conditioning and transmission. This experimental activity is an essential prerequisite for ensuring that the prototype system will generate quality in vivo data when the training database is collected. Knowledge of how each sensor responds in a controlled and standardized environment will enable us to safely interpret in vivo results from the multisensing platform and analyze them by ML-based approaches to produce the assessment of body hydration. The evaluation of variability and sensitivity of the proposed printed sensors, and the standardization of the measurement setups and protocols developed for testing and validating the printed sensors in vitro aim to ensure a fair and repeatable comparison with other future sensors realized by us or other researchers.

The article is organized as follows: preliminary considerations on hydration sensing are introduced in Section II. This is followed in Section III by a general overview of the system and a description of prototype design and fabrication, focusing on printed sensors, analog front-end, transmission interface, and network infrastructure. Finally, Section IV reports on in vitro sensor characterization and details the functional validation of signal conditioning electronics and transmission interface.

II. Hydration Sensing

Among the variety of measurable parameters related to hydration monitoring changes in the electrical properties of the human body are the most directly correlated to the fluctuation of the total body water content. Estimation by impedance analysis has been employed in several works, mostly in the form of whole-body bioelectrical impedance analysis (BIA) requiring specific positioning of electrodes, such as ankle-to-ankle, wrist-to-ankle [8], or single electrodes placed on a wrist [9] or finger [10] together with a single contact placed on the opposite arm to broaden the area of body under test.

Whole-body BIA does not satisfy our requirements for unobtrusive and autonomous operation, which could be met instead by *segmental* BIA, where electrodes are placed over a small area of the body (e.g., within a bracelet), with the advantage of much-reduced sizes and bulk [11]. Despite being convenient in terms of portability, the main problem in such miniaturized BIA systems is that shrinking the measurement on a small volume increases the significance of other physical factors such as temperature, sweat, or moisture due to impaired skin transpiration under the bracelet, thus increasing the contribution of surface currents, that affect measurement as a whole and, in particular, the contact impedance between electrodes and skin. Interference is known to be negligible in whole-body measurements [12], but could have a more significant impact with reduced electrode size [9], the use of a nontranspiring bracelet, and above all, the far reduced volume under test. Yet, although possibly less accurate, segmental BIA is considered a useful tool for body impedance estimation [13]. In view of our aim, we decided to apply segmental BIA to the arm, exploiting multisensing to detect and compensate for impedance variations due to changes in temperature and superficial hydration conditions. Our design relies on a bracelet equipped with a set of printed sensors, as shown in Fig. 1. The four electrodes for tetra-polar BIA are augmented by two other sensing elements, targeting surface information of the subject skin: an interdigitated electrode (IE) providing a sensing area for superficial hydration, and a resistance temperature detector (RTD).

The actual placement of sensors around the arm is illustrated in Fig. 2, with a qualitative indication of relevant electromagnetic field lines. Darker outer layers in the arms cross section represent the skin, the lighter pink part refers to body tissues, and the bone is the middle white part.

Field lines going through all skin and body tissues evidence that BIA can be seen as a 3-D system, whereas interdigitated electrodes cover a 2-D surface portion of limited depth, which evidences their importance in helping discriminate the effect of surface currents. Careful consideration must then be given to the problem of separating the contribution of body hydration from that of skin hydration when impedance is measured.

The measured body impedance can be described by different equivalent circuit models [11]. In the following, the much-simplified circuit of Fig. 3 will be employed since it satisfies completely the level of accuracy required for the analysis proposed. The circuit represents BIA current through the body by the parallel of two paths. The main path is an RC parallel that globally accounts for characteristics of the electrodes, the superficial skin layer, and the deeper tissues. The undesired surface current path due to sweat and surface moisture is modeled by resistance R_{sweat}.

According to this model, the resistive part of the measured body impedance is the parallel between R_{body}, accounting for body hydration, and R_{sweat}, which accounts instead for *skin* hydration. This latter contribution once quantified will have to be compensated since it is influenced mainly by surface sweat and humidity, which do not contribute to the overall body hydration. Changes in skin electrical properties measured thanks to the IE sensor provide additional information regarding sweat rate, environmental humidity, and the specific water content of the skin layers. This information will, therefore, complement the picture provided by BIA electrodes for a more accurate assessment of the *body* hydration status of the subject. As shown in Fig. 4, the equivalent circuit for skin impedance measurement is the series of R_{skin} and of an RC parallel modeling the contact area of the superficial skin patch.

Resistances R_{body}, R_{skin}, and R_{sweat} all vary with water content, and therefore their resistivity must be assumed to vary with the relative water content in the volume of interest,

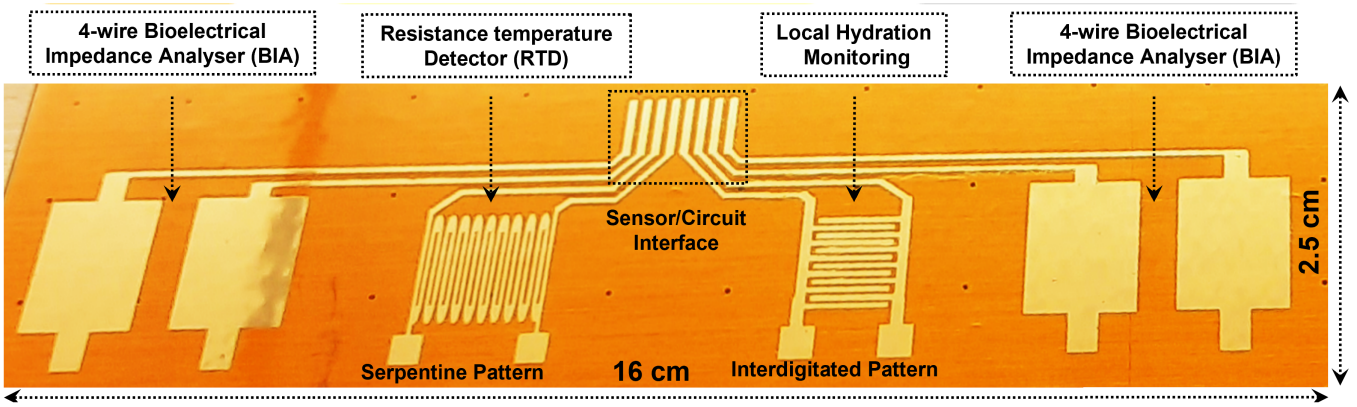

Fig. 1. Inkjet printed multisensing flexible bracelet with serpentine RTD, interdigitated local hydration sensors, and tetra-polar BIA electrodes.

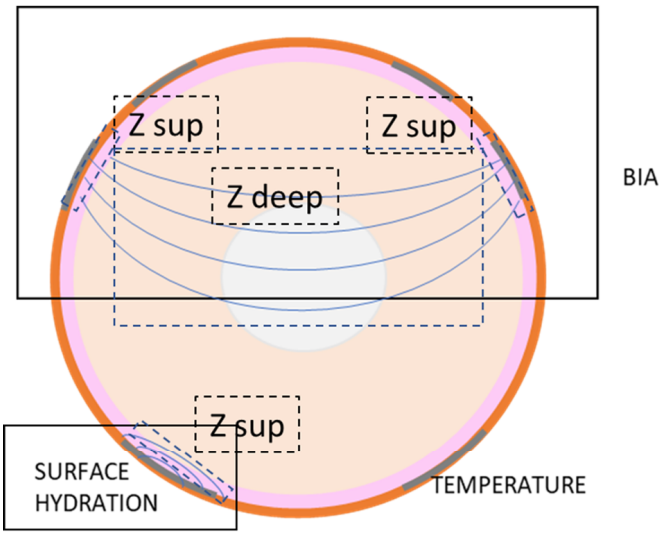

Fig. 2. Sensing with BIA electrodes and interdigitated electrodes (IE)—an illustration of electromagnetic field lines in the arms cross section. Dark outer layers represent the skin, the lighter pink part refers to body tissues, while the bone is represented by the middle white part.

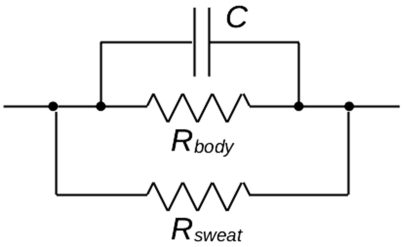

Fig. 3. Equivalent circuit model for BIA impedance.

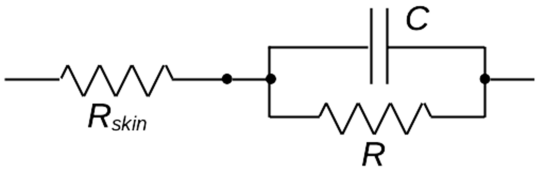

Fig. 4. Equivalent circuit model for surface impedance.

indicated by α. This can be indicated generically by $\rho(\alpha)$, it must be remembered that the value of α for body resistance R_{body} will, in general, differ from those applicable to skin resistances R_{skin} and R_{sweat}.

These simple models allow us to show how resistance measurements obtained by BIA and IE can be combined to improve the estimation of overall body resistance and obtain from that an assessment of body water content. Under the simplifying assumption that skin resistivity is homogeneous (or considering *average* resistivity), measured skin resistance is: $R_{\text{skin}} = \rho(\alpha_{\text{skin}})(l_{\text{IE}}/S_{\text{IE}})$, where $l_{\text{IE}}/S_{\text{IE}}$ is a geometric factor for the IE sensor.

For the total resistance R_{meas} measured by BIA, the component R_{sweat} related to skin surface current will be characterized by an average resistivity similar in value to that of R_{skin}, but, in general, $\alpha_{\text{skin}} \neq \alpha_{\text{body}}$ and the component R_{sweat} affects only a fraction of the BIA sensing volume. One may write

$$R_{\text{sweat}} = \rho(\alpha_{\text{skin}}) \cdot \delta \cdot \frac{l_{\text{BIA}}}{S_{\text{BIA}}} \tag{1}$$

where $l_{\text{BIA}}/S_{\text{BIA}}$ is the geometric factor for the BIA sensor and $\delta < 1$ accounts for the fraction of the sensing volume where the contribution of sweat is significant.

To a first approximation, therefore, one has

$$R_{\text{sweat}} = K \cdot R_{\text{skin}} \tag{2}$$

where K is a factor determined by the geometries of the two hydration sensors in the system

$$K \cong \delta \cdot \frac{l_{\text{BIA}}/S_{\text{BIA}}}{l_{\text{IE}}/S_{\text{IE}}}. \tag{3}$$

More generally, K should be considered to account for all factors related to the sensor layout in the system.

It should be remarked that accurate calibration by this approach would only be possible if an *exact* relationship was known. This short analysis evidences that quantities of interest are indeed related, and motivates our interest in an ML-based approach for elementary-level hydration monitoring, rather than obtaining R_{body} from R_{eq} and R_{sweat} via (2) and (5).

Finally, since temperature is related to changes in both hydration and sweat, the temperature sensor is useful as an indicator of possible effects of the ambient environment on measured impedance values. The local temperature measured by the RTD is influenced by body core temperature, with water content acting as a thermo-regulator. Still, most of all, it depends on environmental temperature, whose variations can affect hydration and, possibly, the performances of conductive

electrodes. Accurate temperature measurements serve as useful feedback when processing the other sensed quantities, to correct and interpret the results obtained. It represents essential information in a multiparametric perspective, contributing useful data for determining the hydration status of a subject [14].

III. System Design and Fabrication

The general architecture for any wearable device typically encompasses three main subsystems: 1) sensing; 2) signal conditioning; and 3) data transmission, as illustrated in Fig. 5. The proposed prototype was designed and extensively tested to demonstrate its functionality as a multisensing device, paving the way to future miniaturization and applicability to in vivo tests. As illustrated in the functional diagram of Fig. 6, system hardware can be divided into seven functional blocks, three of which refer to the RTD analog read-out path.

A. Printed Sensors

Sensor geometries are designed to optimize transduction performances and allow wearability and ease of interfacing with the readout electronics. The specific choice in terms of sensors, dimensions, and positioning of the device results from a combination of the measurement we want to perform (i.e., estimation of hydration level) with the specific requirements imposed by the application target (Fig. 1).

Electrodes for BIA were designed in a tetrapolar configuration, with dimensions for each electrode of 1×1 cm. Four-wire measurement enables compensation for contact resistance, thus achieving accurate results even with reduced-size electrodes, as suggested in the literature [15].

Sensors for skin hydration monitoring were designed with an interdigitated layout and a sensing area of 1 cm^2. This layout is the most sensitive to changes in the skin's electrical properties (i.e., dielectric permittivity and electrical conductivity) caused by small local variations of water concentration in skin tissues.

Body temperature is sensed by an RTD contact temperature sensor. A serpentine pattern was chosen to increase the available sensing surface in a miniaturized area and obtain good sensitivity to temperature changes [16]. The geometry thus compensates for the effects of the complementary materials combined with the conductive ink to allow flexibility, which affects sensitivity as well as produces some nonlinearity in the sensor response.

Inkjet printed technology was selected to fabricate all sensing elements on a flexible bracelet, that can be easily miniaturized and integrated into a wearable device. Compared to screen-printing, inkjet printing offers high-resolution patterning, improved process flexibility, and prevents waste of precious material, being a mask-less drop-on-demand technique [17].

Sensors were realized by a Dimatix DMP 2850 inkjet printer [FUJIFILM Dimatix, Inc., Santa Clara, California (USA)]. A polyimide foil (i.e., Kapton, Dupont) with a thickness of 50 μm was chosen as a substrate. Due to excellent thermal, electrical, mechanical, and chemical properties, this material represents the most suitable candidate for printed electronics applications, enabling optimal ink adhesion during printing and stability after curing [18]. Furthermore, its narrow thickness affords optimal flexibility and conformability to the skin. For all sensors, a silver ink was selected (Sicrys I40DM-106 from PVNanocell, Israel). It is a commercial-engineered conductive ink, based on single-crystal silver nanoparticles in diethylene glycol monomethyl ether (DGME), designed specifically for digital inkjet printing. After printing, all sensors were cured on a hot plate for 30 min at a temperature of 250 °C, as suggested by the ink datasheet, then stored in a glove box until use.

B. Front-End Read-Out Circuitry

The flexible multisensing element integrating BIA electrodes, IE, and RTD was interfaced with custom-designed read-out front-end hardware, designed with particular attention to low-power battery operation, as well as high measurement resolution and sensitivity. Although the prototype circuit was produced on a rigid board for the development stage, the design was specifically thought for ease of miniaturization and migration to a flexible printed circuit-board substrate in future works.

Four-wire and two-wire skin impedance spectroscopy are implemented by a single commercial analog front-end chip (Analog Devices AD5941), that provides a full stand-alone, self-contained measurement system, thereby vastly reducing circuit component count [19]. The chip includes an internal high-precision ac voltage source, that is employed to excite the sensors with a sinewave at a known frequency, superposed to a common-mode bias voltage. The resulting current waveform, after scaling, is recorded by a 16-bit ADC, enabling it to measure sensor impedance and detect its variation by the vector ratio of voltage across the unknown impedance to the current flowing through it. Discrete Fourier transform calculation yields the impedance of real and imaginary parts. Measured values are forwarded to the microcontroller through a serial peripheral interface (SPI) digital line.

Only a few peripheral passive components need to be added to comply with IEC 60601-1 basic safety requirements, as described in the AD5941 datasheet. A pair of capacitors and limiting series resistors, placed close to the chip at each impedance measurement port, provide dc isolation, and limit the maximum allowable current into the human body.

For temperature sensing, the input low-pass (LP) analog filter stage is designed to improve the common-mode rejection ratio (CMRR). Its common-mode and differential-mode bandwidths are $F_{cm} = 16$ kHz and $F_{dm} = 1.5$ kHz, respectively. This is followed by the four-wire RTD sensing unit housing an instrumentation amplifier set to a gain of 1000 and a highly accurate constant RTD current source of 100 ± 0.5 μA (Ref200, Texas Instruments, USA).

The Texas Instruments INA122 instrumentation amplifier is specifically designed for battery-powered applications with the capability of running on a single supply [20]. Its output is further filtered by a sharp roll-off second-order Butterworth LP active filter, based on Sallen–Key topology, with unit gain and cut-off frequency of 1 kHz. A Butterworth filter was preferred due to its smooth frequency response and lack of

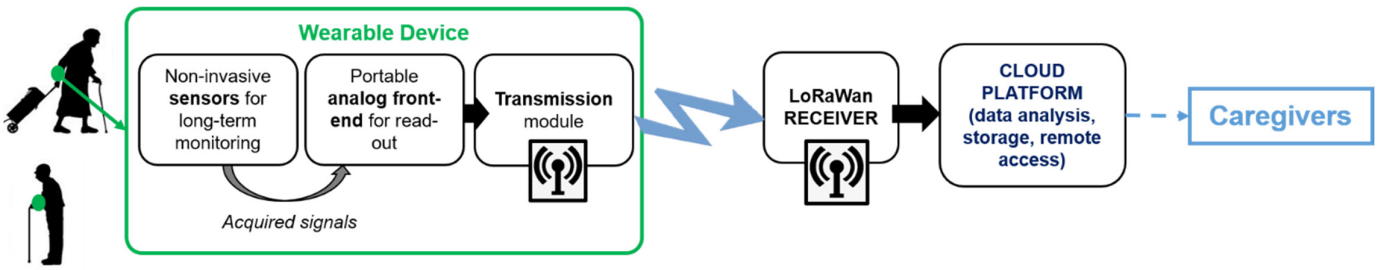

Fig. 5. Scheme representing the general system architecture of the proposed prototype.

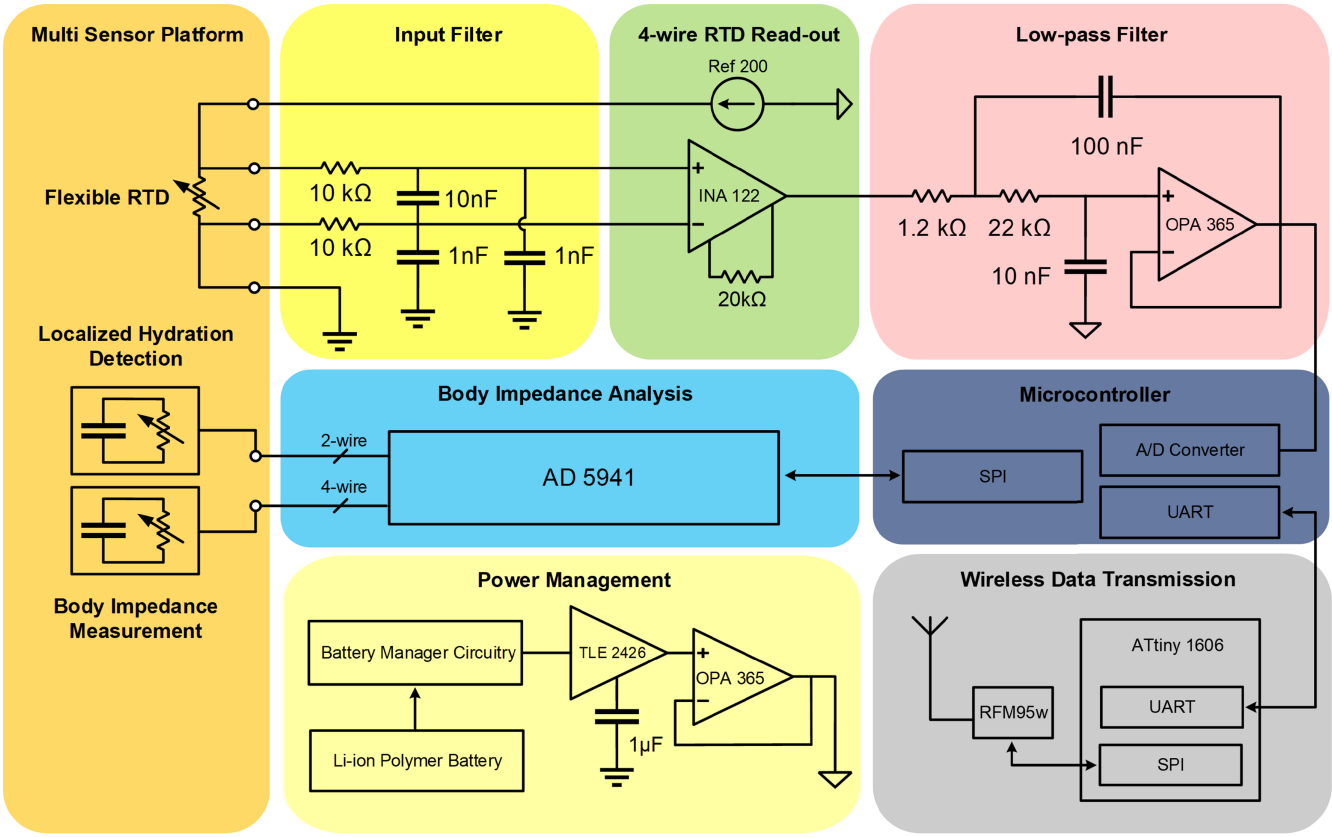

Fig. 6. Overview of the complete device architecture: hardware-level schematic for the sensor read-out front-ends, embedded processor for data acquisition and analysis, LoRaWAN wireless unit for secure low-power medical data transmission.

passband ripple, while Sallen–Key topology was preferred as it requires fewer components. This acts as an anti-aliasing filter for the microcontroller analog to digital converter (ADC) and further removes out-of-band high frequencies. The operational amplifier in the LP filter (Texas Instruments OPA2365) was selected due to its single-supply and rail-to-rail features. As the group delay of the entire read-out chain is negligible it directly translates RTD resistance into voltage at the input of the internal 16-bit ADC to the ST Microelectronics STM32F446 microcontroller, where the actual temperature value is computed.

All circuits are powered by a rechargeable lithium-ion/polymer battery connected to a Microchip MCP73831 single-cell charge management controller. A Texas Instruments TPS61090 dc-dc boost converter and TLE2426 "rail splitter" were employed to provide the required supply voltage and current, with proper virtual ground termination. Additional buffers with higher current ratings were included in the power management unit as a safety margin, in particular, to support the higher peak currents on the RF transceiver. Since RF bursts are very short, this will not have a significant impact on the overall consumption of the unit.

Fig. 6 shows a preliminary block diagram where two different microcontrollers (STM32F446 for data acquisition and ATtiny 1606 for data transmission) are present as a matter of practicality. This enables to split development and characterization of different system blocks during prototype validation but, of course, a single microcontroller is more than enough, and this change will be done in the final revision of the system, leaving only the latter.

C. Data Transmission and Network Infrastructure

The transmitting interface is required to be simple, yet effective, taking into consideration all the constraints arising from the need to monitor subjects in wide areas, and the desire

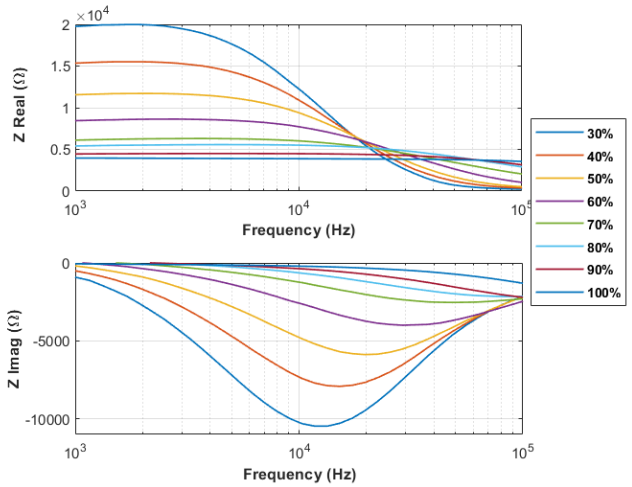

Fig. 7. Response of BIA electrodes to different hydration levels in the frequency range from 1 to 100 kHz.

to avoid reliance on the active use of a mobile phone for data transmission. The latter aspect turns out to be the defining factor in the choice among IoT enabling technologies, as it emphasizes the need for long-range coverage to allow the monitoring of elderly people without hindering their mobility. Long-range (LoRa) modulation and the Low Power Wide Area Network (LoRaWAN) protocol proved to be well-suited, thus being employed for the prototype. LoRaWAN was found to offer a very good tradeoff between LoRa, low power consumption, low hardware cost, and adequate data rates for the application scenario of this work [21]. The protocol is characterized by data rates of 50 kbps at most and allows a fairly limited maximum payload size (no more than 222 or 242 B, depending on the geographic region where the technology is deployed). Since the monitored physical quantities vary slowly over time, neither are constraining for this application scenario.

The core of the wireless data transmission interface is a Microchip ATtiny1606 microcontroller, that is connected via a SPI interface to a HopeRF RFM95w LoRaWAN transceiver. LoRaWAN allows to setting up of an independent, pervasive monitoring infrastructure, ensuring coverage up to some km in a single hop, by which clinicians and caregivers can remotely monitor the hydration levels of patients without requiring them to manage data transmission. The provision of autonomous wireless connectivity thus removes a possible source of error/failure. The transceiver is fit with a $\lambda/8$ whip antenna having a 2 dBi gain. The maximum current drawn during transmission is 80 mA, turning out to be adequate for battery-powered systems [22].

Digitized values measured by the three sensors are sent from the STM32F446 microcontroller to the ATtiny1606 microcontroller via a Universal Asynchronous Receiver Transmitter (UART) interface port. The three sensor readings are arranged into a LoRaWAN packet payload by the ATtiny1606 microcontroller, encrypting them by the Advanced Encryption Standard (AES)-128 exploiting two keys. The packet is then sent to a LoRaWAN gateway, employing a frequency diversity scheme via a frequency hopping technique on eight different channels in the 863–870-MHz ISM band, a spreading factor (SF) seven and bandwidth of 125 kHz. The message queue telemetry transport (MQTT) protocol is employed for forwarding data via the Internet.

The gateway acts as a packet forwarder and conveys the demodulated packets, along with metadata related to reception quality indicators, to the cloud network infrastructure. The remote network infrastructure on the cloud includes an MQTT broker and a network server. It decrypts LoRaWAN packets and then stores all information related to both packet payloads, containing the sensor readings, and quality indicators, related to gateway reception, in a local database. In this way, the network can be monitored and maintained, while data are made available to users and caregivers, in particular, clinicians, for the follow-up of their patients.

IV. System Characterization

A. Printed Sensor Characterization

Printed sensors were characterized in vitro, in a measurable and controlled environment ensuring standardized procedures and repeatable results. Accurate bench-top instrumentation was employed to reduce measurement uncertainty and provide a reference.

Electrodes for BIA analysis were characterized by exploiting a simple test structure mimicking a human arm. Electrodes printed on the polyimide substrates were placed on a layer of synthetic skin-like patch wrapped around a cylindrical sponge, thus replicating the sectional layout of Fig. 3. The acquisition front-end was replaced by a bench-top impedance analyzer (Agilent E4990A, Precision LCR Meter). Different levels of volumetric water content, the typical measurement unit used to indicate hydration status, were set by injecting determined and increasing volumes of water in the sponge with a syringe. As the actual volume of the 3-D setup was 10 cm^3, injection of water in a range from 3 to 10 ml resulted in volumetric water contents ranging from 30% to 100%.

This range of values was selected assuming the average normal ranges of hydration indicated by the clinical literature (50%–65% for males and 45%–60% in females) [23] so that conditions going from severe dehydration (<30%) to hyperhydration (>80%) were represented.

Impedance at different levels of sponge hydration was measured in the frequency range between 1 and 200 kHz with a four-wire layout, like the one employed by the AD5941 analog front end.

Fig. 7 shows the real and imaginary parts of impedance (respectively, Z_{real} and Z_{imag}), plotted versus frequency as measured by the LCR meter. The instrument refers to a series impedance configuration (i e., $Z = R + jX$), that for the circuit model of Fig. 3 has the mathematical expression

$$R + jX = R_{\text{eq}}\left[\frac{1}{1+(\omega R_{\text{eq}}C)^2} + j\frac{\omega R_{\text{eq}}C}{1+(\omega R_{\text{eq}}C)^2}\right] \quad (4)$$

where

$$R_{\text{eq}} = \frac{R_{\text{body}} \cdot R_{\text{sweat}}}{R_{\text{body}} + R_{\text{sweat}}} \quad (5)$$

and C is the sensor capacitance.

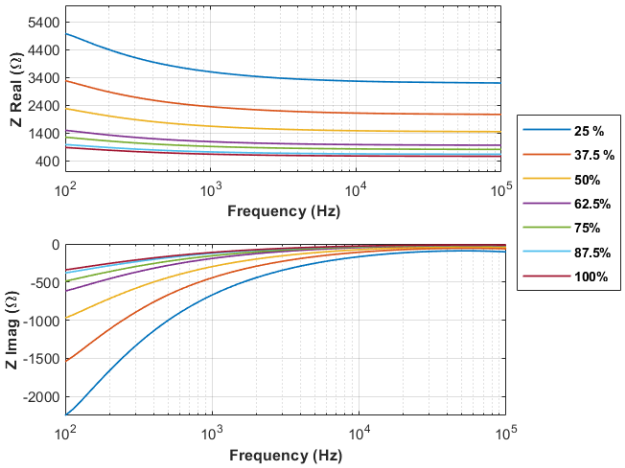

Fig. 8. Response of IE sensors to different hydration levels in the frequency range from 100 Hz to 100 kHz.

Measurements agree with the assumed circuit model and show well the effect of different hydration levels on impedance. As water content increases and R_{eq} decreases accordingly, the reactance peak value occurs at progressively higher frequencies, showing that it is not advisable to refer to reactance for this kind of measurement. However, up to 1 kHz its contribution can be considered negligible (less than 5% of magnitude $|Z|$) in any hydration condition.

IE sensors for skin hydration monitoring were also characterized in a range of simulated skin hydration conditions. In this case, the sensing area was placed over a layer of synthetic skin-like patch injected with controlled volumes of water, ranging from 50 to 200 μl.

Considering a constant volume of 200 mm^3 for the skin-like patch, a range of volumetric water contents going from 25% to 100% were tested, thus including all possible conditions that can be encountered in real scenarios including severe dehydration (<40%), mild dehydration (40% to 50%), normal skin hydration (50% to 70 %), up to hyperhydration or edema (>80%).

Using again the Agilent E4990A Precision LCR Meter, impedance was measured in a frequency range between 100 Hz and 100 kHz, measurements being repeated for six sensor specimens. The plots presented in Fig. 8 are also in the format of an equivalent series impedance $Z = R + jX$, that for the IE equivalent model of Fig. 4 yields the formula

$$R_{\text{skin}} + R\left[\frac{1}{1+(\omega RC)^2} + j\frac{\omega RC}{1+(\omega RC)^2}\right] \tag{6}$$

where R and C are electrical parameters of the interdigitated electrode. Results confirm the ability to discriminate different levels of hydration also in the synthetic skin-like patch. An IE sensor responds to an increase in water content by a decrease in both Z_{real} and the absolute value of Z_{imag}, as shown in Fig. 8, in agreement with the literature [24].

For Z_{real} sensitivity to hydration changes is similar throughout the range of tested frequencies, whereas the contribution of Z_{imag} is higher at the lower frequencies (up to 1 kHz). Although electrode capacitance is significant because of the typical IE geometry, at frequencies of about 10 kHz or higher its contribution is negligible, and measured impedance becomes resistive only, its value practically coinciding with R_{skin}. Figs. 7 and 8 evidence that for our purposes measurements are best taken as Z_{real} at 1 kHz for the BIA sensor and at 10 kHz for the IE sensor.

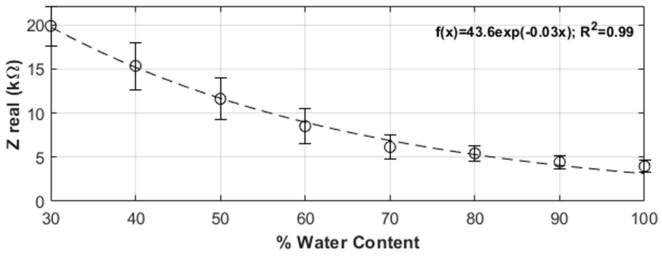

Fig. 9. Calibration of Z_{real} evaluated at 1 kHz for BIA at different volumetric water contents.

Using these plots, it is also possible to compare resistances Req and R_{skin} at common uniform levels of hydration. This provides the opportunity to check our assumption in model (2) by considering ratios of R_{body}(1 kHz) to R_{skin}(10 kHz) at different hydration levels, although in this case $\delta = 1$ in (3), a condition that would hardly occur in practice. The resulting ratio is indeed nearly constant and its average value was found to be 7.8, with a standard deviation of 0.5, which is enough to confirm a proportionality relationship.

Calibration curves were built from characterization plots for Z_{real} similar to those reported in Figs. 7 and 8, obtained for four set of measurements replicated on different sensors. Extremely good results were obtained for both BIA and skin hydration IE using a single-exponential fit, as shown in Figs. 9 and 10, with a value $R^2 = 0.99$ in both cases. The two resulting equations

$$R_{\text{body}} = 43.6\ e^{-0.03\alpha}, \quad \text{and: } R_{\text{skin}} = 8.9\ e^{-0.03\alpha}$$

show that exponential coefficients agree, whereas in this case $R_{\text{body}}/R_{\text{skin}} = 4.9$. The difference from the result above is mostly determined by the limited reproducibility of the 3-D test setup, namely, by the way, the sponge and skin-like patch are assembled. This is not considered an issue, as it actually reflects the real-life situation with monitored subjects. Additional physical features will have to be included among the training inputs for an ML classifier, and these might include the arm circumference where the sensor bracelet will be located and the subject body mass index (BMI). Variability assessed for Z_{real} by a relative standard deviation (RSD) lower than 30% in BIA and than 35% in IE appears significant but acceptable considering the aim of our design and in agreement with RSD values shown by similar BIA analyzers [11] and by studies dealing with IE for hydration sensing [25]. This value can be explained by the contribution of both sensor physical realization and setup construction.

Finally, resistance changes due to temperature (0.04 Ω/°C) within an expected temperature range < 5 °C appear to have negligible influence compared to variations in water volume (hundreds of Ω/%).

Temperature sensors were characterized by means of a hot plate with manual temperature control. To ensure a more homogeneous heat distribution, a layer of synthetic skin-like

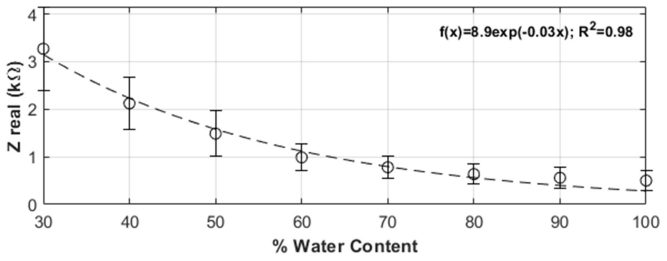

Fig. 10. Calibration of Z_{real} evaluated at 10 kHz for IE sensors at different volumetric water contents.

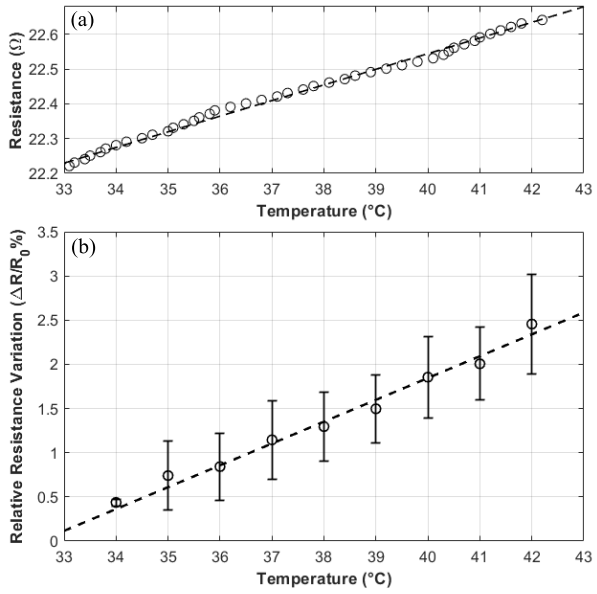

Fig. 11. Response of temperature sensors to temperature variations. (a). Response of a single sensor to temperature variation: sample time 10 s, sensitivity 0.044 Ω/°C, and $R^2 = 0.99$. (b) Average transfer characteristic of six sensors to change in steady-state temperature: sensitivity of $0.247 \pm 0.056\%/°C$, TCR of 0.002, and $R^2 = 0.99$.

patch was placed between the sensor and the hot plate. The temperature on the patch surface in contact with the RTD was measured by a commercial thermometer (Hanna Instruments HI 98 501 Digital Thermometer [26], accuracy 0.3 °C, and resolution 0.1 °C). The resistance between the terminals of the serpentine RTD was measured using a benchtop multimeter (Keysight Technologies, 34401A Digital Multimeter, six-digit resolution).

In a preliminary test, the response of a single sensor was evaluated while the temperature was changing rapidly, in a physiological range typically experienced on the surface of the skin. To enable rapid and controlled temperature variation, the sensor was attached to a hot plate, the temperature control of the plate was switched from room temperature to 45 °C, and as soon as the temperature of the plate reached 32 °C, plate temperature, and RTD resistance were simultaneously recorded every 10 s, in the range between 32 °C and 42 °C. This experiment provided the temperature to resistance transfer characteristic reported in part A of Fig. 11, that shows good linearity ($R^2 = 0.99$) and a sensitivity of 0.044 Ω/°C.

To investigate variability six different printed sensor specimens were tested in the range of temperatures between 33 °C and 42 °C with temperature steps of 1 °C. At each step,

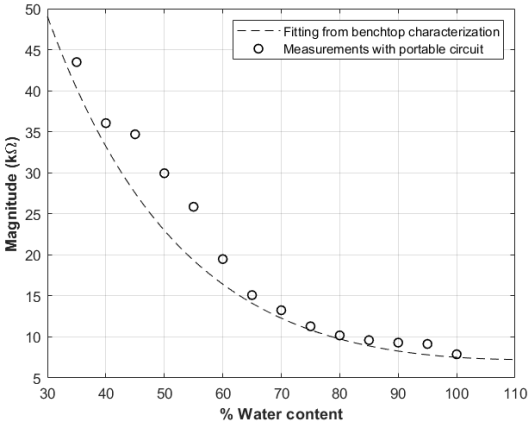

Fig. 12. Response of four-wire BIA obtained with the portable read-out circuit.

resistance was measured after the temperature reached a steady state. All sensors showed a linear characteristic ($R^2 = 0.99$) with average sensitivity, in terms of absolute resistance values, of 0.039 ± 0.015 Ω/°C. The variability observed among sensor units (RSD = 38%) can be mainly related to process variability that characterizes fast prototyping sensor fabrication, as highlighted in a recent literature review for printed resistive sensors [17], and to some degree of variability in the setup assembly.

Relative resistive variation is plotted in part B of Fig. 11 instead of absolute resistance values, to better highlight the common trend. Here, the average sensitivity is $0.247 \pm 0.056\%/°C$ and the average RSD is reduced to 22%. The corresponding value of the temperature coefficient of resistance (TCR) is 0.0025, which appears in agreement with the literature on printed temperature sensors [27].

B. Read-Out Circuits

Tests where sensor read-out electronics were included replicated the experiments reported in the previous Section. For BIA electrodes, the same 3-D test setup previously detailed in Section IV-A was used, where the human arm is mimicked by a synthetic skin-like patch wrapped around a cylindrical sponge. Controlled hydration levels ranging from 20 to 200 μl/cm^2 with steps of 10 μl/cm^2 were obtained by injecting increasing volumes of deionized (DI) water. After allowing sufficient time to reach a uniform water distribution within the material, the four BIA electrodes in the bracelet were connected to the read-out electronics, and impedance values were recorded at a frequency of 1 kHz. These were acquired for 30 s, then averaged to obtain one point in the calibration curve (Fig. 12).

To validate the IE sensor, controlled hydration levels between 10 and 200 μl/cm^2 were likewise obtained by injecting DI water into the skin-like patch. Impedance was recorded by the two-wire read-out circuit after each injection at a frequency of 100 Hz, at steps of 10 μl/cm^2, for 30 s, then averaged to obtain one point in the calibration curve (Fig. 13).

Results obtained, in both cases, show trends that agree with those obtained during the printed sensors characterization activity described in Section IV-A. As the sensor transfer characteristics are nonlinear, higher sensitivities are

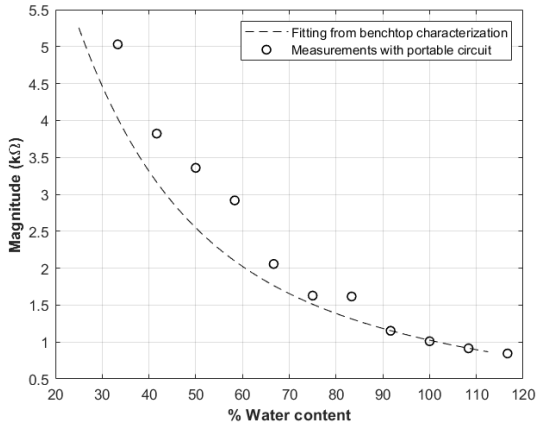

Fig. 13. Response of two-wire impedance measurement for the skin hydration IE sensor obtained with the portable read-out circuit.

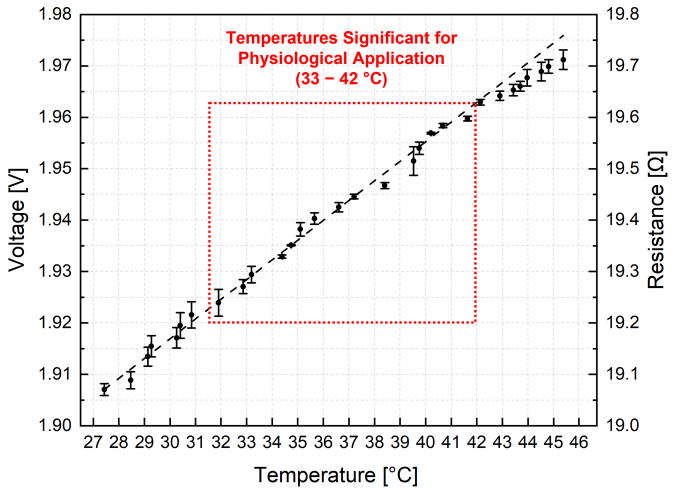

Fig. 14. Response of four-wire RTD front-end connected to the flexible temperature sensor in a dynamic experiment where the temperature changed swiftly from 27 °C to 45 °C in ∼30 s. The $R2$ value is 0.9973, sensitivity is 0.0384 Ω/°C, CV is 11.93%, and three measurements were recorded to compute the error bars.

obtained at lower hydration levels (below 60 μl/cm^3 for BIA and 60 μl/cm^2 for skin hydration), whereas saturation can be observed at the higher hydration levels (higher than 160 μl/cm^3 for BIA and 140 μl/cm^2 for skin hydration). This means sensitivity gets better when dehydration is approached, which fits with the aims of the system.

The temperature read-out chain for the flexible RTD was calibrated using an ultrastable PI controller (WTC3243HB, Wavelength Electronics, USA) was acquired and coupled to a thermoelectric cooler (TEC 1.4-6, Thorlabs, USA), and a commercial (TH10K, Thorlabs, USA) negative temperature coefficient thermistor (NTC). The flexible RTD was connected to the read-out chain we developed and placed on the TEC, which is connected to the PI controller and the NTC to complete the control loop. The set temperature of TEC was programed via the PI controller to step up quickly (in ∼30 s) from 27 °C to 45 °C. Then, both the sensed temperature values from the RTD front end and the reading from the commercial NTC were recorded in a triplicated experiment. A very good linear range ($R^2 = 0.9973$) was achieved with sensitivity of 0.0384 Ω/°C, TCR of 0.00272, and RSD of 12% (Fig. 14).

C. Transmission Validation

System validation was completed by a second test assessing overall system functionality, including the transmitting interface. The test was performed in the laboratory by forwarding the digitized values coming from the read-out electronics during the validation measurement campaign to the network infrastructure. The LoRaWAN gateway is a Dragino LG308, which is a multichannel gateway capable of receiving and demodulating up to 8 LoRaWAN packets at the same time even if they were broadcast exploiting different SFs on multiple channels. Gateway sensitivity varies depending on the adopted transmission parameters, and in this case (i.e., SF = 7 and bandwidth 125 kHz) it reaches values down to −126 dBm, thus hinting at the LoRa coverage capability. The gateway is provided with the same type of antenna as the LoRaWAN transceiver of the transmitting interface.

The transmitting interface sampled data with a sampling period of 10 s, then sent information related to the three sensors via LoRaWAN. The network infrastructure on the cloud converted the digitized values into the related sensor measurements. Since the test was carried out in a laboratory, no packet loss occurred. In the light of experience from previous works (e.g., [28]), the same outcome is highly likely also when the receiver is remotely placed (e.g., hospitals). Nonetheless, for this application, even a moderate loss of packets can be tolerated, since measured physical quantities are slowly varying over time [29], [30].

Within its application scenario, the proposed system will not perform continuous transmission due to two main reasons: 1) targeted parameters are not changing very rapidly over time, thus a transmission period of, for example, 30 min would be enough and 2) applications enabled by LoRaWAN protocol must abide by regional regulations related to fair usage of frequency bands [31], limiting temporal occupancy to 1% (at least in Europe). An extended interval between transmissions is beneficial from the point of view of power consumption, translating into an increase in battery lifetime.

This test aimed to assess the proper operation of the transmission interface and the network infrastructure, and therefore its duration was only limited to 500 s, transmitting data with an interval of 10 s. Test results confirmed that the transmission interface and the network infrastructure implement transparent transfer of data.

V. Conclusion

This article aims to propose and characterize in vitro a proof-of-concept prototype of a multisensing device for monitoring hydration, integrating flexible printed sensors, portable electronics, and a LoRaWAN transmitting interface. Characterization of the low-cost printed multisensing bracelet showed that each sensor can detect controlled changes in the targeted variable in vitro. Testing performed with the customized electronics showed the ability to reproduce the same experiments performed with bench-top instrumentation, with good accuracy and repeatability. Finally, integration testing of the electronic read-out circuits with the transmission module confirmed the possibility of effectively transmitting a package of data from

the three sensors every 10 s, which is satisfactory for real-time hydration monitoring.

Results obtained with the prototype discussed in this article represent a promising start in the development of a fully miniaturized device, to be tested and employed in a real-life application scenario. Future work will focus on in vivo characterization of the printed sensors to test variability and reproducibility and on the acquisition of different targeted parameters in different hydration conditions.

An essential step to enable an ML approach will consist of adequately training the algorithm for which gathering a suitable training dataset is necessary. During this phase, the ordinal scale will be employed to associate proper labels to the different hydration levels acquired during in vivo acquisition tests. This will be an essential part since publicly available databases hardly exist and, in any case, they would not be specific to the proposed sensor configuration. The full working prototype here developed will enable the acquisition of reliable and robust training information.

REFERENCES

[1] A. M. El-Sharkawy et al., "Dehydration and clinical outcome in hospitalised older adults: A cohort study," *Eur. Geriatric Med.*, vol. 8, no. 1, pp. 22–29, Feb. 2017.

[2] A. Cataldo et al., "Portable microwave reflectometry system for skin sensing," *IEEE Trans. Instrum. Meas.*, vol. 71, pp. 1–8, 2022.

[3] A. J. Bandodkar et al., "Battery-free, skin-interfaced microfluidic/electronic systems for simultaneous electrochemical, colorimetric, and volumetric analysis of sweat," *Sci. Adv.*, vol. 5, no. 1, Jan. 2019, Art. no. eaav3294.

[4] D. Solovei, J. Žák, P. Majzlíková, J. Sedláč ek, and J. Hubálek, "Chemical sensor platform for non-invasive monitoring of activity and dehydration," *Sensors*, vol. 15, no. 1, pp. 1479–1495, Jan. 2015.

[5] H. C. Ates et al., "End-to-end design of wearable sensors," *Nature Rev. Mater.*, vol. 7, no. 11, pp. 887–907, Jul. 2022.

[6] R. Sokullu, M. A. Akkaş, and E. Demir, "IoT supported smart home for the elderly," *Internet Things*, vol. 11, Sep. 2020, Art. no. 100239.

[7] A. Galli, G. Giorgi, C. Narduzzi, G. Peruzzi, A. Pozzebon, and S. Tonello, "IoT technologies for active ageing: An overview of the elderly dehydration case," in *Proc. IEEE Int. Symp. Med. Meas. Appl.*, Jun. 2022, pp. 1–6.

[8] B. J. Thomas, B. H. Cornish, L. C. Ward, and M. A. Patterson, "A comparison of segmental and wrist-to-ankle methodologies of bioimpedance analysis," *Appl. Radiat. Isot.*, vol. 49, nos. 5–6, pp. 477–478, May 1998.

[9] M. H. Jung et al., "Wrist-wearable bioelectrical impedance analyzer with miniature electrodes for daily obesity management," *Sci. Rep.*, vol. 11, no. 1, p. 1238, Jan. 2021.

[10] M. Usman, A. K. Gupta, and W. Xue, "Analyzing dry electrodes for wearable bioelectrical impedance analyzers," in *Proc. IEEE Signal Process. Med. Biol. Symp. (SPMB)*, Dec. 2019, pp. 1–5.

[11] S. Abasi, J. R. Aggas, G. G. Garayar-Leyva, B. K. Walther, and A. Guiseppi-Elie, "Bioelectrical impedance spectroscopy for monitoring mammalian cells and tissues under different frequency domains: A review," *ACS Meas. Sci. Au*, vol. 2, no. 6, pp. 495–516, Dec. 2022.

[12] B. H. Cornish, B. J. Thomas, and L. C. Ward, "Effect of temperature and sweating on bioimpedance measurements," *Appl. Radiat. Isot.*, vol. 49, nos. 5–6, pp. 475–476, May 1998.

[13] P. Deurenberg, M. Deurenberg-Yap, and F. Schouten, "Validity of total and segmental impedance measurements for prediction of body composition across ethnic population groups," *Eur. J. Clin. Nutrition*, vol. 56, no. 3, pp. 214–220, Mar. 2002.

[14] F. Sabry, T. Eltaras, W. Labda, F. Hamza, K. Alzoubi, and Q. Malluhi, "Towards on-device dehydration monitoring using machine learning from wearable device's data," *Sensors*, vol. 22, no. 5, p. 1887, Feb. 2022.

[15] P. Kassanos, F. Seichepine, and G.-Z. Yang, "A comparison of front-end amplifiers for tetrapolar bioimpedance measurements," *IEEE Trans. Instrum. Meas.*, vol. 70, pp. 1–14, 2021.

[16] D. Barmpakos and G. Kaltsas, "A review on humidity, temperature and strain printed sensors—Current trends and future perspectives," *Sensors*, vol. 21, no. 3, p. 739, Jan. 2021.

[17] P. Bellitti, M. Borghetti, E. Cantu, E. Sardini, and M. Serpelloni, "Resistive sensors for smart objects: Analysis on printing techniques," *IEEE Trans. Instrum. Meas.*, vol. 71, pp. 1–15, 2022, doi: 10.1109/TIM.2022.3181941.

[18] S. Diaham, "Polyimide in electronics: Applications and processability overview," in *Polyimide for Electronic and Electrical Engineering Applications*. London, U.K.: IntechOpen, 2021, ch. 1.

[19] R. Harder, A. Diedrich, J. S. Whitfield, M. S. Buchowski, J. B. Pietsch, and F. J. Baudenbacher, "Smart multi-frequency bioelectrical impedance spectrometer for BIA and BIVA applications," *IEEE Trans. Biomed. Circuits Syst.*, vol. 10, no. 4, pp. 912–919, Aug. 2016.

[20] A. J. Golparvar and M. K. Yapici, "Toward graphene textiles in wearable eye tracking systems for human–machine interaction," *Beilstein J. Nanotechnol.*, vol. 12, pp. 180–189, Feb. 2021.

[21] G. Peruzzi, A. Galli, and A. Pozzebon, "A novel methodology to remotely and early diagnose sleep bruxism by leveraging on audio signals and embedded machine learning," in *Proc. IEEE Int. Symp. Meas. Netw.*, Jul. 2022, pp. 1–6.

[22] A. Lombardo, S. Parrino, G. Peruzzi, and A. Pozzebon, "LoRaWAN versus NB-IoT: Transmission performance analysis within critical environments," *IEEE Internet Things J.*, vol. 9, no. 2, pp. 1068–1081, Jan. 2022.

[23] W. C. Chumlea, S. S. Guo, C. M. Zeller, N. V. Reo, and R. M. Siervogel, "Total body water data for white adults 18 to 64 years of age: The fels longitudinal study," *Kidney Int.*, vol. 56, no. 1, pp. 244–252, Jul. 1999.

[24] R. AlDisi, Q. Bader, and A. Bermak, "Hydration assessment using the bio-impedance analysis method," *Sensors*, vol. 22, no. 17, p. 6350, Aug. 2022.

[25] S. Ramanathan et al., "Elastomeric polydimethylsiloxane polymer on conductive interdigitated electrode for analyzing skin hydration dynamics," *Appl. Phys. A*, vol. 126, no. 9, pp. 1–11, Sep. 2020.

[26] *Hanna Instruments, Hi 98501 Digital Thermometer Parameters*. Accessed: Jan. 17, 2023. [Online]. Available: https://docs.rs-online.com/2c8a/0900766b8136831b.pdf

[27] Q. J. Liew, A. S. A. Aziz, H. W. Lee, M. W. Lee, H. F. Hawari, and M. H. M. D. Khir, "Inkjet-printed flexible temperature sensor based on silver nanoparticles ink," *Eng. Proc.*, vol. 2, no. 1, p. 3, Nov. 2020.

[28] L. Parri, S. Parrino, G. Peruzzi, and A. Pozzebon, "A LoRaWAN network infrastructure for the remote monitoring of offshore sea farms," in *Proc. IEEE Int. Instrum. Meas. Technol. Conf.*, May 2020, pp. 1–6.

[29] G. S. Kelly, "Body temperature variability (Part 2): Masking influences of body temperature variability and a review of body temperature variability in disease," *Alternative Med. Rev.*, vol. 12, no. 1, pp. 1–14, 2007.

[30] H. M. Logan-Sprenger and L. L. Spriet, "The acute effects of fluid intake on urine specific gravity and fluid retention in a mildly dehydrated state," *J. Strength Conditioning Res.*, vol. 27, no. 4, pp. 1002–1008, 2013.

[31] (2020). *LoRa Alliance, LoRaWAN 1.0.1 Regional Parameters*. Accessed: Jan. 17, 2023. [Online]. Available: https://hz137b.p3cdn1.secureserver.net/wp-content/uploads/2020/11/rp_2-1.0.1.pdf?time=1673563697

Sarah Tonello (Member, IEEE) received the M.S. degree (cum laude) in biomedical engineering from the University of Florida, Gainesville, FL, USA, and Politecnico di Milan, Milan, Italy, in 2014, as part of the dual degree program Atlantis CRISP. She received the Ph.D. degree in technology for health from the University of Brescia, Brescia, Italy, in 2017.

During the Ph.D. and Post-Doctoral, she has performed several periods abroad as a Visiting Researcher with the Integrated Circuit Laboratories of Prof. Sandro Carrara, EPFL, Lausanne, Switzerland. Now she is a Researcher with the Department of Information Engineering, University of Padua, Padua, Italy. Her research interests include printed sensors, electronic devices, and electrochemical sensors.

Alberto Zacchini received the bachelor's and M.S. degrees in biomedical engineering from University of Padua, Padua, Italy, in 2020 and 2023, respectively. With a strong academic background and a deep-rooted interest in technology, he is pursuing his career exploring for his own the fascinating intersection of AI and healthcare, specifically focusing on the application of deep-learning models in EEG portable devices.

He is currently working as a Product Specialist at ASA Laser, Nogarazza, Italy, with key responsibilities related to product development. He is also involved in a Startup project named MIND AID as a Product Developer of a wearable EEG device.

Alessandra Galli (Member, IEEE) received the B.Sc. and M.Sc. degrees in biomedical engineering and the Ph.D. degree in information and communication technology from the School of Information Engineering with a dissertation about IoT measurements for long-term monitoring applications, University of Padua, Padua, Italy, in 2015, 2017, and 2021, respectively.

From 2021 to 2022, she was a Post-Doctoral Researcher with the Instrumentation and Measurements Group, University of Padua. In September 2023, she joined Eindhoven University of Technology (TU/e), Eindhoven, The Netherlands, as a Post-Doctoral Researcher supported by a Marie Skłodowska-Curie Postdoctoral Fellowship. Her research interests include biomedical signal processing, compression and anomaly detection, and machine learning.

Ata Golparvar (Member, IEEE) received the Bachelor of Science degree from the Azad University, Tabriz, Iran, in 2016, and the Master of Science degree in electronics from Sabanci University, Istanbul, Türkiye, in 2019.

He is now with the Bio/CMOS Interfaces Laboratory in EPFL Neuchatel, Lausanne, Switzerland. His research interests include soft devices and wearable technologies.

Ali Meimandi (Graduate Student Member, IEEE) received the B.Sc. degree in electrical engineering from the Amirkabir University of Technology (Tehran Polytechnic), Tehran, Iran, and the M.Sc. degree in electronic engineering from Politecnico di Milan, Milan, Italy, in 2018 and 2022, respectively. He is currently pursuing the Ph.D. degree with the BioCMOS Interfaces (BCI) Laboratory, École Polytechnique Fédérale de Lausanne, Lausanne, Switzerland.

His research is focused on designing and implementing ultralow power and ultralow area analog/mixed-signal IC for brain monitoring. His current research interests include biosensors, neural prostheses, analog and digital CMOS design, ultralow power, and miniaturized CMOS integrated circuits to develop innovative biomedical systems.

Giacomo Peruzzi (Member, IEEE) received the B.Sc. degree in information engineering, the M.Sc. degree in computer and automation engineering, and the Ph.D. degree in information engineering and science from the University of Siena, Siena, Italy, in 2016, 2019, and 2023, respectively.

He is a Research Fellow with the Instrumentation and Measurements Group, University of Padua, Padua, Italy. His current research interests include the fields of the Internet of Things (IoT) and distributed measurement systems. In particular, he deals with wireless sensor networks (WSNs) for monitoring systems that are enabled by low-power wide-area network (LPWAN) technologies, as well as embedded machine learning (ML) for measurement infrastructures.

Alessandro Pozzebon (Senior Member, IEEE) received the M.Sc. degree in information engineering, with a focus on the radio frequency identification (RFID) technology applied to cultural heritage, and the Ph.D. degree from the University of Siena, Siena, Italy, in 2006 and 2012, respectively.

He is currently an Assistant Professor with the Department of Information Engineering, University of Padua, Padua, Italy, where he teaches with the Laboratory of Electronic Measurements. His main research interests include the development of applications based on low-power wide area networks (LPWAN), wireless sensor networks (WSN), and RFID technologies in several different application fields, from healthcare to cultural heritage and environmental monitoring.

Nicolò Lago (Member, IEEE) received the bachelor's degree in information engineering, the master's degree in electronic engineering, and the Ph.D. degree in information engineering from the University of Padua, Padua, Italy, in 2012, 2014, and 2017, respectively.

He is currently working as an Electrical Technician with Ecoprogetti SRL, Carmignano di Brenta, Italy, working on the research and development of test equipment for solar cells and panels. His research interests include the characterization and modeling of organic thin-film transistors for biochemical applications and the modeling and reliability of polymeric and perovskite solar cells for next-generation green electronics.

Andrea Cester (Senior Member, IEEE) received the M.S. degree in electronic engineering and the Ph.D. degree in electronic and telecommunication engineering from the University of Padua, Padua, Italy, in 1998 and 2002, respectively.

He is currently an Associate Professor with the Department of Information Engineering, University of Padua. He is the author/coauthor of more than 200 articles published in international journals and conference proceedings. His research activities range from the characterization, reliability study, and modeling of organic electronic devices, photovoltaic devices, graphene-based TFT, and organic biosensors.

Giada Giorgi (Member, IEEE) received the Laurea degree in telecommunications engineering and the Ph.D. degree in microelectronics and telecommunications engineering from the University of Padua, Padua, Italy, in 2003 and 2007, respectively.

She is currently an Associate Professor with the Department of Information Engineering, University of Padua. Her research activities are in the field of distributed measurement systems and signal processing. They include the development of measurement applications for wireless sensor and actuator networks (WSAN), wireless body sensor networks (WBN), and cyber-physical systems (CPS), and the analysis and development of synchronization algorithms.

Dr. Giorgi is a member of the IEEE TPC-37 (Measurement and Networking).

Sandro Carrara (Fellow, IEEE) is currently a Faculty Member with EPFL, Lausanne, Switzerland, and a former Professor with the University of Genoa, Genoa, Italy, and the University of Bologna, Bologna, Italy. Throughout his career, he published seven books, with prestigious publishers like Springer/Nature and Cambridge University Press. He has published 400 articles and holds 17 patents.

Dr. Carrara was a member of the Board of Governors of the IEEE Circuits and Systems Society (CASS). He is also a member of the Executive Committee of the IEEE Sensors Council. He was a recipient of the IEEE Sensors Council Technical Achievement Award. He is the Editor-in-Chief of the IEEE SENSORS JOURNAL and an Associate Editor of IEEE TRANSACTIONS ON BIOMEDICAL CIRCUITS AND SYSTEMS.

Claudio Narduzzi (Life Member, IEEE) received the Laurea degree in electronics engineering from University of Padua, Padua, Italy, in 1982.

He is currently a Full Professor in instrumentation and measurement with the Engineering School, University of Padua. His research interests encompass several instrumentation-related application areas in electronics, telecommunications, and networking. Current activities are mainly oriented toward networked and IoT-based measurement systems, the analysis of their performances, and the application of advanced signal-processing methods, such as compressed sensing, in distributed measurement.

Prof. Narduzzi is an IEC representative in the JCGM Working Group on the International Vocabulary of Basic and General Terms in Metrology (VIM).

Open Access funding provided by 'Università degli Studi di Padova' within the CRUI CARE Agreement